Monthly Notices of the ROYAL ASTRONOMICAL SOCIETY

MNRAS **503,** 1036–1050 (2021) doi:10.1093/mnras/stab343
Advance Access publication 2021 February 6

Twin stars as tracers of binary evolution in the *Kepler* era

Sara Bulut [1]★ Barış Hoyman [1] Ahmet Dervişoğlu [2,3] Orkun Özdarcan [1,4] and Ömür Çakırlı [1]

[1]*Science Faculty, Astronomy and Space Science Deptartment, Ege University, Bornova, İzmir 35100, Turkey*
[2]*Department of Astronomy and Space Sciences, Erciyes University, Kayseri 38039, Turkey*
[3]*Astronomy and Space Sciences Observatory and Research Center, Erciyes University, 38039, Kayseri, Turkey*
[4]*TÜBİTAK National Observatory, Akdeniz University Campus, 07058, Konyaaltı, Antalya, Turkey*

Accepted 2021 February 1. Received 2021 February 1; in original form 2020 November 24

ABSTRACT

We present results of the combined photometric and spectroscopic analysis of four systems that are eclipsing binaries with a twin component (mass ratio $q \simeq 1$). These are exceptional tools to provide information for probing the internal structure of stars. None of the systems were previously recognized as twin binaries. We used a number of high-resolution optical spectra to calculate the radial velocities and later combined them with photometry to derive orbital parameters. Temperatures and metallicities of systems were estimated from high-resolution spectra. For each binary, we obtained a full set of orbital and physical parameters, reaching precision below 3 per cent in masses and radii for whole pairs. By comparing our results with PARSEC and MIST isochrones, we assess the distance, age, and evolutionary status of the researched objects. The primary and/or secondary stars of EPIC 216075815 and EPIC 202843107 are one of the cases where asteroseismic parameters of δ Sct and γ Dor pulsators were confirmed by an independent method and rare examples of the twin-eclipsing binaries therefore the following analyses and results concern the pulsating nature of the components.

Key words: binaries: eclipsing – binaries: spectroscopic – stars: evolution – stars: fundamental parameters – stars: late-type.

1 INTRODUCTION

In the studies of eclipsing binaries, how unique the eclipsing binaries with twin components (mass ratio $q \simeq 1$) is in comparison to other systems is one of the most compelling yet elusive questions. Several such systems containing a twin-type component have been recently found (Tokovinin 2000; Lombardi et al. 2011; El-Badry et al. 2019).

The earliest statistical investigation of binary stars with known mass ratios was performed by Lucy & Ricco (1979). In the same study, they investigated the formation mechanisms of different groups of stars. Furthermore, Tokovinin (2000) studied the role of multiple systems in the formation scenario, for twin binaries accompanied at least one distant third body. According to the early work done on statistical twin binaries studies, twins are found in the range of spectral type K2 to F8. The first statistical study on mass ratio–probability density of twin binaries (q–N) was done by Halbwachs et al. (2003), by taking spectral type into account. In the same study, they concentrated on the mass ratio distribution of spectroscopic binaries of F–G and K spectral types and also determined that these three spectral types demonstrated a similar distribution except for small discrepancies.

Recently, investigations on the mass ratio distributions of binary stars (e.g. Lucy 2006; Simon & Obbie 2009) point out that the proportion of eclipsing binaries with twin components with a mass ratio of q = 0.98–1.00 is around 3 per cent and that F, G, and K spectral types are dominant. The statistical relations indicated that low mass twins are often found in binary star populations where the rate of star formation is slower. For this reason, it is clear that the determination of F, G, and K spectral types among twin binary stars will contribute in general to the understanding of star formation and in particular to the understanding of the formation of two stars with the same characteristics and testing of current star formation models.

To explore any more, it is inevitable to study some twin binaries in more detail. The main purpose of our work is in line with this principle; calculation of the fundamental parameters of components of twin eclipsing binary systems, through their precision light and radial velocity curve analysis, description of their evolutionary status, and stellar atmospheric model investigation. With these newly investigated systems, we are now at a point where we can determine the grade to which twin binaries are physically identical or fraternal, thereby testing the theoretical explanation on forming twins and fundamental assumptions.

The rest of this paper is organized as follows. In Section 2, we briefly discuss the literature information about the targets, and in Section 3 we describe how we acquired and processed photometric and spectroscopic data and explain our radial velocity extraction process, light-curve analysis, and how we obtained atmospheric parameters from disentangled spectra where we calculated each star's light contribution to the spectra to perform stellar atmosphere modelling. We then present evolutionary status of the systems in Section 4. This paper also demonstrates new pulsating components in eclipsing binary systems, based on precise, nearly continuous, and long-time-base *Kepler* data. Section 5 presents in detail the analysis of their pulsation spectrums. Finally, detailed conclusions are presented in Section 6.

★ E-mail: sb.sarabulut@gmail.com

Table 1. Literature information about the targets from this work.

EPIC	Common name	RA (deg)	DEC (deg)	P (d)[a]	T_0 (BJD-2450000)[a]	K_p(mag)	d (pc)
202843107	2MASS J16221147-2809426	245.548	−28.162	2.1988862[b]	6894.3025[b]	11.829	551.7(29.8)[d]
204321014	–	15.964	−22.796	3.7927310[c]	6898.3491[c]	12.426	391.2(2.6)[d]
216075815	TYC 6874-632-1	288.042	−23.006	3.9959011[b]	7303.7313[b]	11.743	813.1(8.3)[d]
217988332	TYC 6306-1822-1	292.699	−19.609	6.4906817[b]	7301.8176[b]	11.129	906.6(14.1)[d]

[a]For the eclipsing binary, where T_0 is the primary eclipse mid-time; [b](Prša et al. 2011; http://keplerebs.villanova.edu/); [c](Barros, Demangeon & Deleuil 2016); [d]From *Gaia* eDR3 parallaxes (Gaia Collaboration 2016, 2020)

2 TARGETS

Our targets were identified as potential twins by visual inspection of the detrended light curves drawn from publicly available *Kepler* Eclipsing Binary Catalog – Third Revision by Kirk et al. (2016). We downloaded the light-curve data from the web site[1] and used a simple PYTHON code to plot the data for each system while making a note of any stars showing eclipse-like features in the light curve. Among these light curves to find twins we used a very simple method. If a binary has two identical components in terms of mass, radius, and temperature properties, their light curves should have very similar primary and secondary eclipses. Therefore, eclipsing binary light curves with similar eclipses are picked to be the initial twin candidates. The list of stars selected for further analysis is shown in Table 1 together with some basic characteristics and their ephemerides of the systems. The *K2* light curves for all eclipsing binaries are depicted in Fig. 1. For each of them we briefly present the basic information below.

EPIC 202843107 is listed as an eclipsing binary candidate in the second campaign field of the *K2* mission. In fact the system was first identified as an exoplanet candidate by Vanderburg & Johnson (2014). On the other hand, Armstrong et al. (2016) classified the system as an eclipsing binary using the machine learning technique. Barros et al. (2016) also pointed out its binary nature by analyzing the de-correlated flux position of the photometric pixel file. Finally, Ou, Yang & Zhou (2019) reported that the system has two stars that have similar radii and one of them is a δ Sct variable.

EPIC 204321014 is the faintest star in our sample according to the measured K_p magnitude (Barros et al. 2016). There is no apparent V magnitude of the target in the literature. This star is classified as a variable star in Kirk et al. (2016). Other than brightness and position measurements, no literature data is available and no light-curve solutions or radial velocity studies have been attempted so far.

EPIC 216075815 is listed as an eclipsing binary candidate system with a period of ∼3.99 d by Huber et al. (2016). Out-of-eclipse variations in the system light curves are noticeable. Except brightness (apparent V magnitude: $11^m.59$) and position measurements (Høg et al. 2000), no literature data is available and no light-curve solutions or radial velocity studies have been attempted so far.

EPIC 217988332 is the longest period system in this study (P ≃ 6.49 d). This star is listed in the *K2* Variable Catalogue (Huber et al. 2016) as an eclipsing binary, but no period estimate is given. Its apparent V magnitude is $10^m.27$ (Høg et al. 2000), and the amplitudes of photometric variations are remarkable. Even though the target appears in Maxted & Hutcheon (2018), no spectroscopic or photometric solution is presented in the literature so far.

[1]http://keplerebs.villanova.edu/

3 DATA AND ANALYSIS

3.1 *K2* photometry

The main purpose of the *Kepler* and the reinvented *K2* tasks (Borucki et al. 2010; Howell et al. 2014) are to detect and define characteristics of the planets by possessing high signal to noise ratio (S/N) time-series photometry of planetary transit of host stars. Up to now, *K2* has completed observing 19 campaigns. In this study, we focused on the search for twin binaries during complete *K2* campaigns that includes numerous types of systems. We downloaded the target pixel files pertaining to the systems from the MAST[2] database. Subsequently, we produced our own masks and using the KEPEXTRACT routine inside the PYKE tools (Still & Barclay 2012) we have extracted the light-curve for each system.

3.2 Spectroscopic data

We queried the ESO Science Archive Facility,[3] looking for optical spectra with a resolution high enough to detect the lines of the binary components in the composite spectrum. Analysed targets in this study have been observed multiple times in order to search for Cepheids as primary distance indicators in the Gaia era[4] therefore we found a number of spectra that showed a good orbital phase distribution for each target. We retrieved HARPS archival data for our targets listed in Table 1. The preference for ESO 3.6-metre telescope (R ≃ 80 000, in EGGS mode) at the *La Silla Observatory* in Chile is motivated by its characteristics: large wavelength range (the optical spectral region from ∼3800 to ∼6900 Å in only one exposure), high resolution, and high spectral stability, which makes it suitable for detecting narrow absorption features in a wide variety of spectral lines (see appendix Table A1).

3.3 Orbital solutions

For the radial velocity measurements, we used our own templates for the implementation of the RAVESPAN technique (Pilecki et al. 2013, 2015). It is capable of working in three methods for the velocity determination from the implemented spectra. These are simple cross-correlation method (CCF; Simkin 1974; Tonry & Davis 1979), two-dimensional cross-correlation (Mazeh & Zucker 1994), and the broadening function technique (Rucinski 2002).

In order to measure velocities we used the cross-correlation method implemented in the RAVESPAN application with template spectra matching the target and its companion in the temperature gravity plane (further information regarding generating synthetic

[2]This can be obtained from https://archive.stsci.edu/
[3]http://archive.eso.org/cms.html
[4]Based on spectra from observations made with ESO telescopes at La Silla Observatory under programmes 099.D-0380(A) and 0100.D-0273(A) by Gieren, W. and 0101.D-0697(A) by Pietrzynski, G.

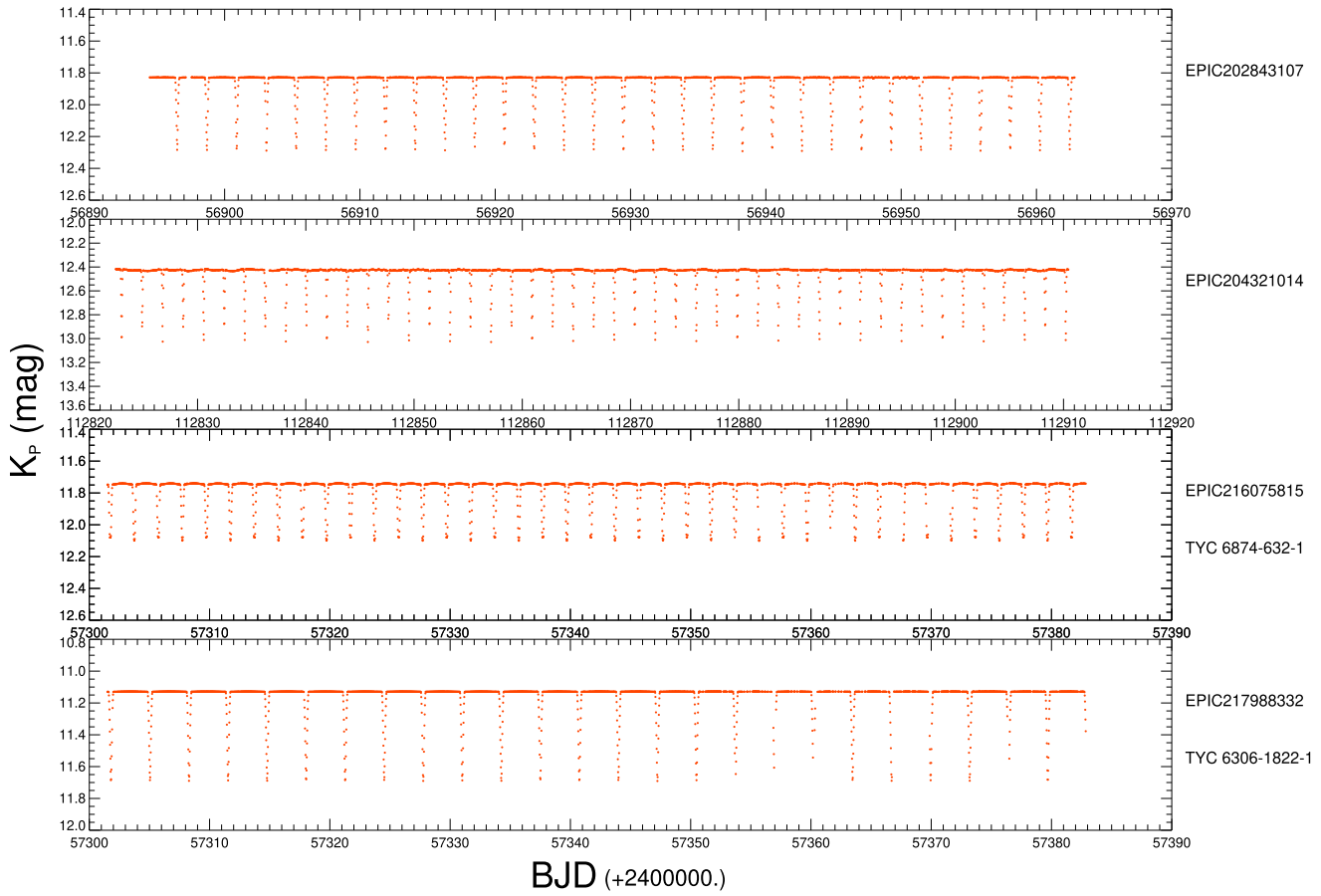

Figure 1. Gallery of *K2* light curves for twin like eclipsing binaries in *Kepler* field. At the right of each panel, EPIC ID number, and common name of the systems are shown. Note that the all light curves downloaded from the archive.

spectra is given in Section 3.5). Radial velocities were measured in the large range 4000–6800 Å. The typical formal errors of the velocities of the system components are about 0.3 km s^{-1}. Fig. 2 displays examples of CCFs at various orbital phases for the systems. The two peaks, non-blended, correspond to each component of the systems. The stronger peaks in each CCF in Fig. 2 correspond to the more luminous component that has a larger weight in the observed spectrum. We adopted a two-Gaussian fit algorithm to resolve cross-correlation peaks near the quadratures when spectral lines are visible separately. At this phase, absorption lines of the primary and secondary components of the system can be easily recognized in the range between 4300 and 6800 Å. These regions include the following lines: He I 4387 Å, Mg II 4481 Å, He I 4713 Å, He I 5016 Å, He I 4917 Å. We limited our analysis in the spectral domains in the range that includes several photospheric absorption lines. We have disregarded very broad lines like H_α, H_β, and H_γ because their broad wings affect the CCF and lead to large errors. Following the method proposed by Penny et al. (2001) we first made two-Gaussian fits of the well-separated CCFs using the deblending procedure. The average fitted full width at half-maximums (FWHMs) are measured for the primary and secondary components. Indeed, the shapes and velocities corresponding to the peaks of the CCFs are slightly changed. By measuring the areas enclosed by the Gaussian profiles of the spectral lines belonging to the primary (A_1) and secondary (A_2), we estimate the light ratio of the primary star (F_1) to the secondary (F_2). This way, we were able to obtain an estimate of the monochromatic flux ratio in the red and blue part of the spectra of $F_1/F_2 \sim A_1/A_2$ 1.00 ± 0.12 for EPIC 202843107, 1.04 ± 0.16 for EPIC 204321014, 1.17 ± 0.21 for EPIC 216075815, and 1.08 ± 0.14 for EPIC 217988332 based on the relative line depths of the spectral components.

The measured FWHMs of the components are the weighted averages of the values obtained from the cross-correlation of strong absorption lines of the target spectra with the corresponding lines of the standard star spectrum. The weight $W_i = 1/\sigma_i^2$ has been given to each measurement. The standard errors of the weighted means have been calculated on the basis of the errors (σ_i) in the FWHM values for each line according to the usual formula (e.g. Topping 1972). The σ_i values are computed by FXCOR according to the fitted peak height, as described by Tonry & Davis (1979).

Our study relies predominantly on a spectroscopic dataset obtained with the HARPS spectrograph. Altogether individual spectra of the eclipsing binaries were cross-correlated against synthetic spectra. We present orbital solutions in Fig. 3 with the radial velocities O–C diagrams that show that our residuals are phased to our solution. The final parameters and their uncertainties are given in Table 2 that contains the binary ID, date of periastron passage (T_0), the orbital period (P), the eccentricity (e), argument of periastron (ω), radial velocity of the center-of-mass (γ), and the orbital amplitude of the components ($K_{1,2}$). The resultant heliocentric radial velocities for the primary (V_1) and the secondary (V_2) components are listed in Table A1, along with the dates of observations. The σ_i values are computed according to the fitted peak height, as described by Tonry & Davis (1979).

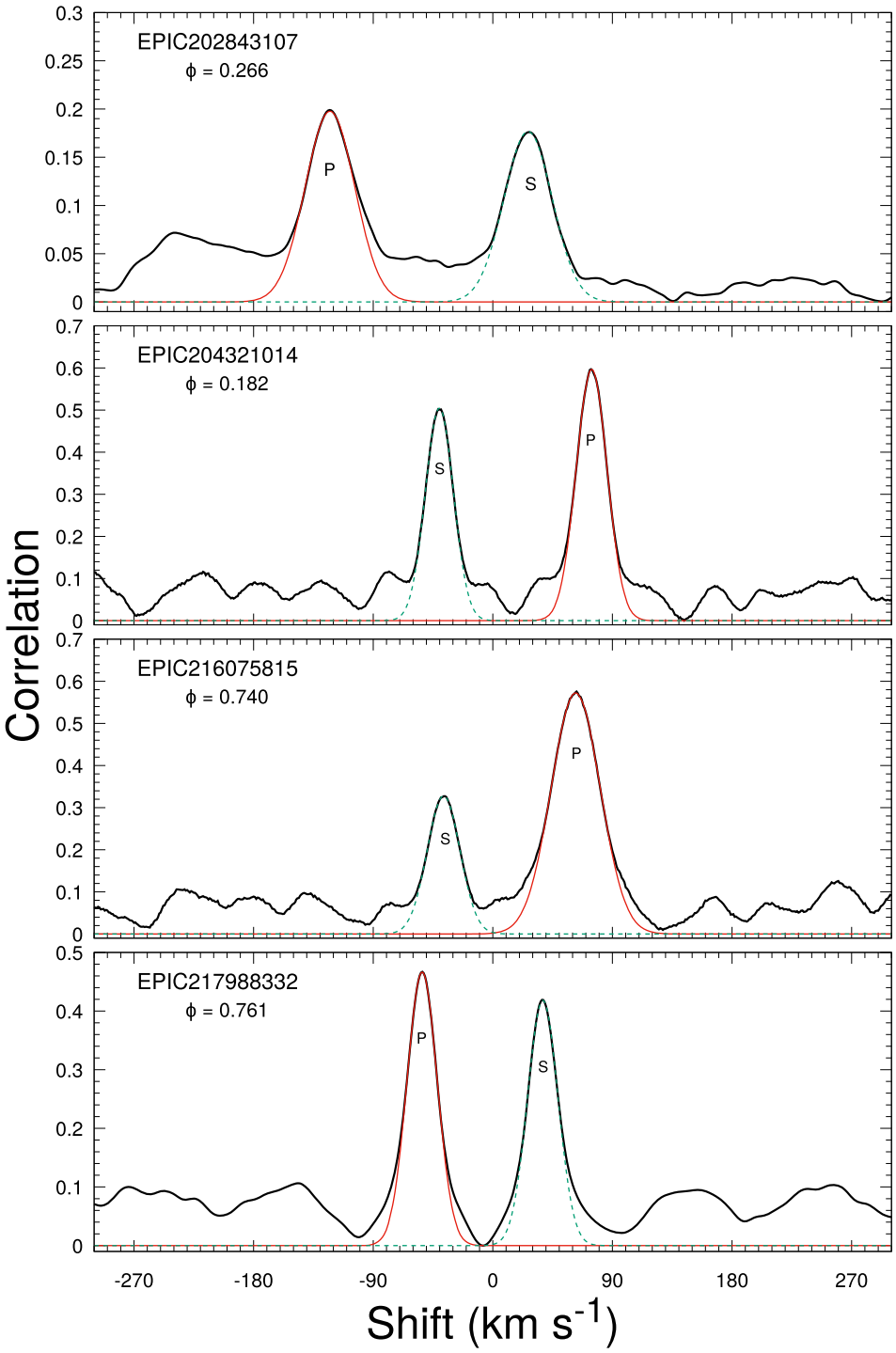

Figure 2. Sample of CCFs between observed specra and synthetic template spectra at the phases that given in subplots.

3.4 Light-curve modelling

The light curves of target systems show typical features of Algol-type binaries as seen in their shapes. Spherical or slightly ellipsoidal components in binaries make it possible to specify, for their light curves, the beginning and ending moments of the eclipses with high accuracy. Furthermore, between eclipses, the light remains almost constant or varies too little to be measured with receivers because of reflection effects, slightly ellipsoidal components, or physical variations. Between the eclipses, light amplitudes are also quite different and may reach several milimagnitudes. These stars are relatively faint, with *Kepler* magnitudes of 12–14. We requested only long cadence data, with integration time per data point of 29.4 min.

To investigate the eclipsing nature in detail, we applied the PHOEBE (v0.32 SVN; Prša & Zwitter 2005), which is a graphical front-end interface to the Wilson–Devinney method (Wilson &

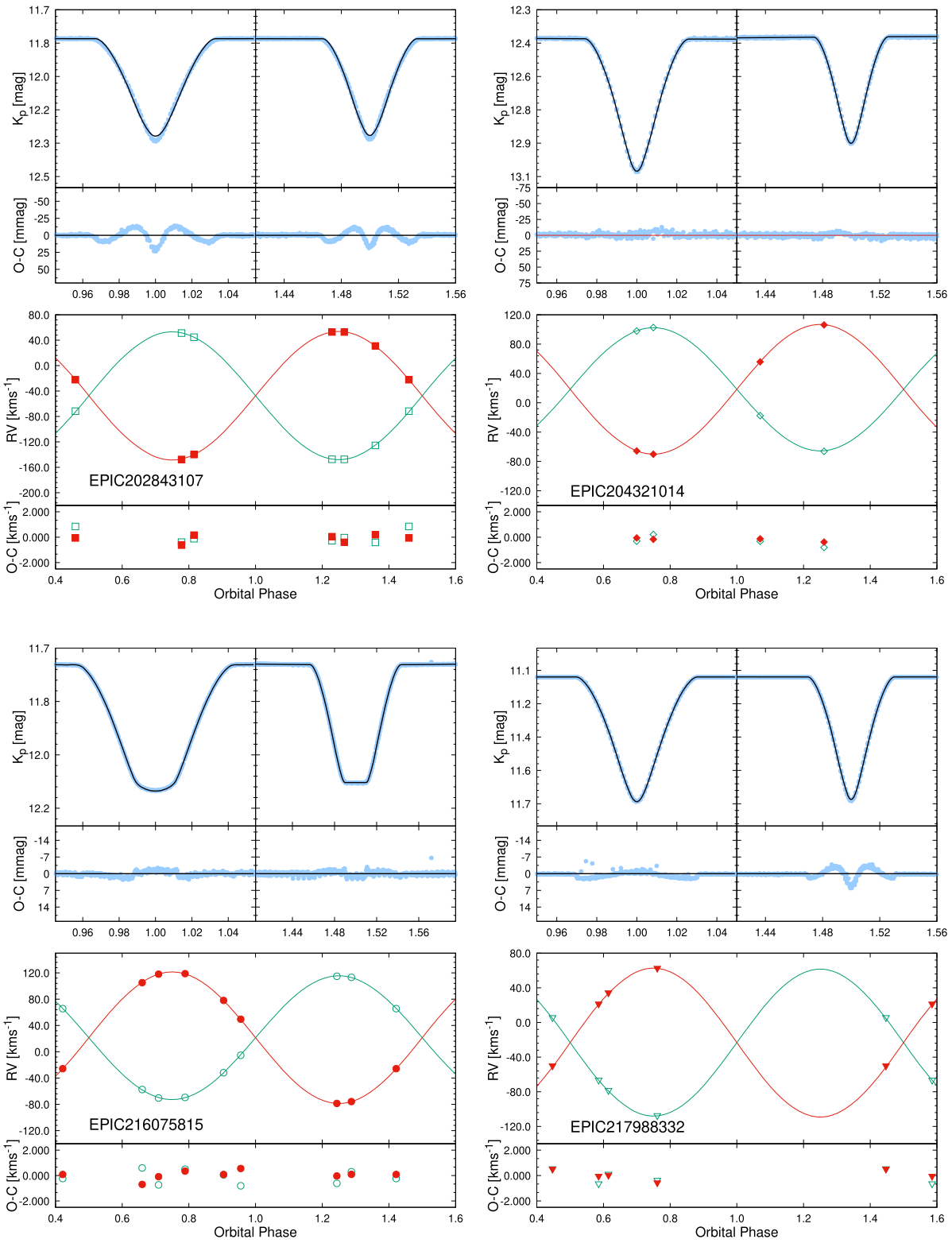

Figure 3. Joint fits to the *K2* photometry and radial velocity time series of target stars. The upper left-hand and right-hand panels show the primary and secondary eclipses, respectively. The best-fitting models are plotted with continuous lines. Filled symbols on the radial velocity plot refer to the primary, and open symbols to the secondary. The light curve model is fitted to the complete K_p-band *Kepler* photometry light curves. Phase '1.0' is for the deeper eclipse mid-time.

Table 2. Binary parameters of systems. Errors in units of the last digits are given in parentheses. $l_1/(l_1+l_2)$, M_{bol}, $(m–M)_V$, and d denote luminosity ratio, absolute bolometric magnitude, distance modulus, and distance, respectively.

Parameter	EPIC 202843107		EPIC 204321014		EPIC 216075815		EPIC 217988332	
	Primary	Secondary	Primary	Secondary	Primary	Secondary	Primary	Secondary
PHOEBE analysis								
T_0 (HJD−2400 000)[a]	56 894.2958(4)		58 035.4919(3)		57 303.7363(6)		57 301.8096(19)	
P (d)	4.397801(1)		3.792131(1)		3.995916(1)		6.490683(1)	
$a \sin i$ ($R_\odot$)	17.52(9)		12.89(4)		15.49(9)		21.88(7)	
γ (km s^{-1})	-47.41(44)		18.36(1)		21.36(25)		-23.24(21)	
$K_{1,2}$ (km s^{-1})	100.6(8)	101.1(8)	83.9(7)	88.1(8)	97.4(2)	99.2(2)	84.8(3)	85.9(3)
e	0.001(1)		0.002(1)		0.002(1)		0.001(2)	
ω (rad)	1(1)		3(1)		6(1)		3(3)	
q	0.995(10)		0.952(6)		0.979(10)		0.987(6)	
i(°)	86.84(1)		88.17(8)		87.88(1)		88.13(6)	
$T_{eff\,1,2}$ (K)	8 000[fix]	7 990(110)	5 800[fix]	5 561(110)	7 000[fix]	7 074(120)	7 500[fix]	7 495(160)
$\Omega_{1,2}$	11.338(20)	10.868(16)	12.749(18)	12.985(19)	6.759(13)	10.163(24)	11.3877(114)	11.4902(116)
$A_{1,2}$	1.0[fix]	1.0[fix]	0.5[fix]	0.5[fix]	1.0[fix]	1.0[fix]	1.0(fix)	1.0(fix)
$g_{1,2}$	1.0[fix]	1.0[fix]	0.32[fix]	0.32[fix]	1.0[fix]	1.0[fix]	1.0[fix]	1.0[fix]
$X^b_{1,2}$	0.6072	0.6076	0.6656	0.6787	0.6236	0.6223	0.6164	0.6166
$Y^b_{1,2}$	0.439	0.861	0.5090	0.4910	0.744	0.256	0.5733	0.4267
$l_1/(l_1+l_2)$	0.51		0.55		0.58		0.52	
$r_{1,2}$	0.1191(2)	0.1131(3)	0.0848(3)	0.805(4)	0.1224(2)	0.0991(3)	0.0991(4)	0.0928(7)
$\Sigma W(O-C)^2$	0.0101		0.099		0.0097		0.0099	
ISPEC analysis								
$T_{eff\,1,2}$ (K)	8 000(150)	7 770(180)	5 800(180)	5 750(250)	7 000(120)	6 850(220)	7 500(200)	7 350(220)
log ($g_{1,2}$) (cgs)	4.28(77)	4.32(65)	4.41(21)	4.43(23)	4.01(16)	4.15(15)	4.14(33)	4.25(43)
$v_{mic.\,1,2}$ (km s^{-1})	2.02	3.31	0.81	1.01	1.28	1.29	2.12	3.01
$v_{mac.\,1,2}$ (km s^{-1})	6.06	5.89	2.43	2.73	5.92	4.90	4.00	4.79
$(v_{1,2}\sin i)_{obs}$ (km s^{-1})[c]	27.5(5)	29.3(7)	10.2(8)	11.4(8)	25(2)	25(4)	13.3(9)	11.5(1.1)
[M/H]	−0.06(5)	−0.05(8)	0.21(9)	0.19(7)	0.01(10)	0.02(11)	−0.07(7)	−0.11(9)
Reduced χ^2	0.012	0.031	0.016	0.041	0.09	0.031	0.027	0.031
Absolute parameters								
$M_{1,2}$ ($M_\odot$)	1.88(3)	1.87(4)	1.03(4)	0.98(4)	1.58(3)	1.55(3)	1.68(3)	1.66(4)
$R_{1,2}$ ($R_\odot$)	2.09(2)	1.98(2)	1.09(4)	1.04(4)	1.90(1)	1.54(9)	2.17(4)	2.03(2)
log ($g_{1,2}$) (cgs)	4.07(3)	4.11(3)	4.37(2)	4.39(3)	4.08(3)	4.26(3)	3.99(7)	4.04(8)
log ($L_{1,2}/L_\odot$)	1.207(32)	1.161(54)	0.087(45)	−0.018(77)	0.892(37)	0.709(62)	1.128(58)	1.070(81)
$(v_{1,2}\sin i)_{calc}$ (km s^{-1})[d]	24.4(1.1)	22.8(1.3)	14.5(9)	13.9(1.0)	24.1(1.3)	19.5(1.5)	16.9(7)	15.8(5)
$M_{bol\,1,2}$ (mag)	1.730(82)	1.847(136)	4.531(112)	4.797(194)	2.520(94)	2.978(155)	1.929(146)	2.074(203)
$(m–M)_V$ (mag)	9.395(115)		8.584(117)		9.513(121)		9.233(123)	
$E(B-V)$[e] (mag)	0.024(9)		0.030(7)		0.040(11)		0.020(5)	
d (pc)[f]	757(19)		521(12)		799(13)		933(14)	
$d^g_{(Gaia)}$ (pc)	552(30)		391(3)		813(8)		907(14)	

[a]Mid-time of the primary (deeper) eclipse, calculated from the complete light curve. [b]X and Y, linear and non-linear coefficients of limb darkening, respectively. [c]It is $v_{1,2}$ calculated with ISPEC. [d]It is the velocity of (pseudo) synchronous given by JKTABSDIM . [e]The $E(B-V)$ values derived from Na I (D_1 & D_2). [f]The JKTABSDIM distance is calculated only when both values of T_{eff} were found with ISPEC. [g]From *Gaia* eDR3 parallaxes.

Devinney 1971; Wilson 1979) to model the light curves and to determine the photometric solutions of the four binary systems. The code modeled light curves with powerful heuristical minimization algorithms, a flexible scripting facility, and an intuitive graphical user interface.

During the synthesis, effective temperature of the hotter primary component was set to be fixed, which we defined from the atmosphere analysis of the systems explained in the next section. The monochromatic (X, Y) limb-darkening coefficients were interpolated from the tables of Sing (2010). The gravity-darkening exponents were fixed at standard values of g_1 and g_2 (Lucy 1967; Ruciński 1969), while the bolometric albedos at A_1 and A_2 (see Table 2). Furthermore, a synchronous rotation ($F_{1,2} = 1.0$) for both components was adopted and the reflection treatment was applied. The adjustable parameters became the orbital ephemeris (T_0, P), the system velocity (γ), the semi–major axis (a), the mass ratio (q), the orbital inclination (i), the surface temperature (T_2) of the secondary component, the dimensionless surface potentials ($\Omega_{1,2}$) of the components, and the monochromatic luminosity (L_1). After more iteration, we determined that, for *K2* data, the uncertainty coming from using slightly inaccurate limb-darkening coefficients does not significantly influence the final errors of solution-based parameters.

Fig. 3 illustrates that the configurations of our binary modelling provided an agreement fit to the light and radial curves, and it allowed us to define the absolute dimensions of systems (see further sections). The agreement between light and radial velocity analysis is acceptable in the error range and the precision of derived parameters has been much improved. However, a small inconsistency in the light-curve analysis of EPIC 202843107 and EPIC 217988332 may be the result of the asymmetric maxima of light curves. Furthermore, an eclipsing binary system has a number of basic physical quantities that will affect the shape of its light curve.

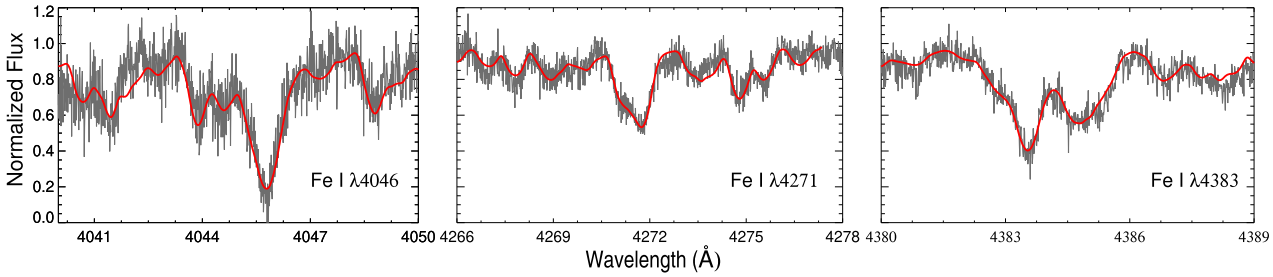

Figure 4. Three spectral portion of the primary component of EPIC 216075815. The dark grey lines represents the disentangling spectrum obtained by the FDBINARY code. The red line represent the synthetic spectra of 7100, 7000, and 7120 K, respectively, interpolated from the atmosphere model of the Kurucz (1993), where log $g_1 = 4.0$ and [Fe/H] = 0.0.

Light and radial curve analysis results are given at the top of Table 2, where the radii are the mean volume radii computed from the tables of Mochnacki (1984). The luminosity (L) and bolometric magnitudes (M_{bol}) were derived by adopting $T_{eff,\odot} = 5\,780$ K and $M_{bol,\odot} = +4.73$ for solar values.

3.5 Atmospheric parameters from disentangled spectra

To understand the nature and detailed spectroscopic analysis of the twin binaries, we planned to figure out the fundamental atmospheric parameters, abundances which we need to investigate the evolutionary status of the components, and the projected rotational velocity (*vsini*) values of the component stars of the systems. Following the analysis of the radial velocity and light-curve analysis, the atmospheric parameters were acquired from the disentangled spectra.

To shed more light on the disentangling of the binary spectra, we prefer the FDBINARY[5] code. The code uses the technique of spectral disentangling (Simon & Sturm 1994) formulated in *Fourier* space (Hadrava 1995) and enforced in the FDBINARY code (Ilijic et al. 2004) in order to separate the individual spectral contributions for the binary systems. The code is also capable of three-component disentangling, as well as light ratio variations by phase. As we have explained below, the only basis in this study is the calculation of light ratio changes of the two components with respect to the orbital phase. The application of the procedure bypasses the step of radial velocity determination but simultaneously optimizes orbital elements of the system and individual spectra of the binary components instead. Furthermore, this is known to introduce spurious low-frequency oscillations in the disentangled spectra (Hensberge, Ilijić & Torres 2008) that were presumably removed in the plots.

In the runs, we employ the disentangling of several (typically two or three) spectral regions where the contributions from both binary components can be clearly visible and determine orbital elements from each of the considered regions separately. Among the several spectral regions, we focused on the spectral interval of 5100–5200 Å because it has been well known for a long time that strong lines with marked wings can be useful tracers of the log g parameter (Gray 2005). We also did some trials to get robust effective temperatures and projected rotational velocity of the components. To get temperatures and projected velocities, we choose three absorption lines that manifest themselves on their spectra; Fe I λ4046, Fe I λ4271, and Fe I λ4383. These lines are useful temperature indicators for the dwarf stars as noted in the Gray & Corbally (2009). By way of example, Fig. 4 demonstrates the disentangled spectrum from the FDBINARY code, together with three synthetic spectra of 7100, 7000, and 7120 K for the primary component of EPIC 216075815. We also used the initial input parameters (the epoch T_0, the orbital period P, the eccentricity e, the longitude of periastron ω, and semi-amplitudes $K_{1,2}$) calculated from our orbital solution and light-curve modelling in previous sections. The subscripts 1 and 2 denote the primary and secondary components, respectively. Then we applied the disentangling technique to the selected spectral regions to obtain the pure spectrum of each star to be used for the atmospheric analysis.

The resulting disentangled spectra of the primary and secondary component are plotted in Fig. 5. After the disentangled spectra of each spectral part were obtained, they were re-normalized considering the average light ratio of components obtained from the initial light-curve analysis and measured light contributions over spectral lines. In this process, the procedure given by Ilijic (2004) was used.

The main goal of this work was to obtain atmospheric parameters that are essential to derive very precisely the age and evolutionary status of the twin binary components, from the pure spectrum of each component. This would be possible by combining the orbital parameters derived from radial velocities with the photometric parameters calculated by precise light-curve analysis in previous sections. Despite its apparent simplicity, as we will explain in results, although the spectral data is sensitive, combining it with the *K2* data turned out to be very challenging.

In order to corroborate for the estimation of stellar parameters given in Table 2, we used the freely available, PYTHON-based code ISPEC (the Integrated SPECtroscopic framework; Blanco–Cuaresma et al. 2014) to verify the primary and secondary stellar parameters. To maintain the atmospheric parameters, we used the spectral synthesis approach, where the key drivers are employing the code SPECTRUM (Gray & Corbally 1994), the MARCS grid of model atmospheres (Gustafsson et al. 2008), and solar abundances from Grevesse, Asplund & Sauval (2007), and atomic line list provided by the third version of the Vienna Atomic Line Database (VALD3; Ryabchikova et al. 2015). ISPEC synthesizes spectra only in certain, user-defined ranges, called 'segments' that plays an integral role in analysis and is defined as regions of 100 Å around a certain line. We run the fit with the following parameters set free: effective temperature T_{eff}, gravity log g, metallicity [M/H], and rotational velocity $v \sin i$ using a set of spectra spread over the orbital period at known times. The resolution R was always fixed to 80 000. Lines of systems are quite narrow, so macro- and microturbulence velocities v_{mic}, v_{mac} were automatically calculated by ISPEC from an empirical relation found by Sheminova (2019) and incorporated into the ISPEC program.

The full optimized parameters are listed in Table 2. The result of an application of this disentangling procedure is illustrated in Fig. 5 for the 5 150–5 200 Å region. This figure shows separated spectra

[5]http://sail.zpf.fer.hr/fdbinary/

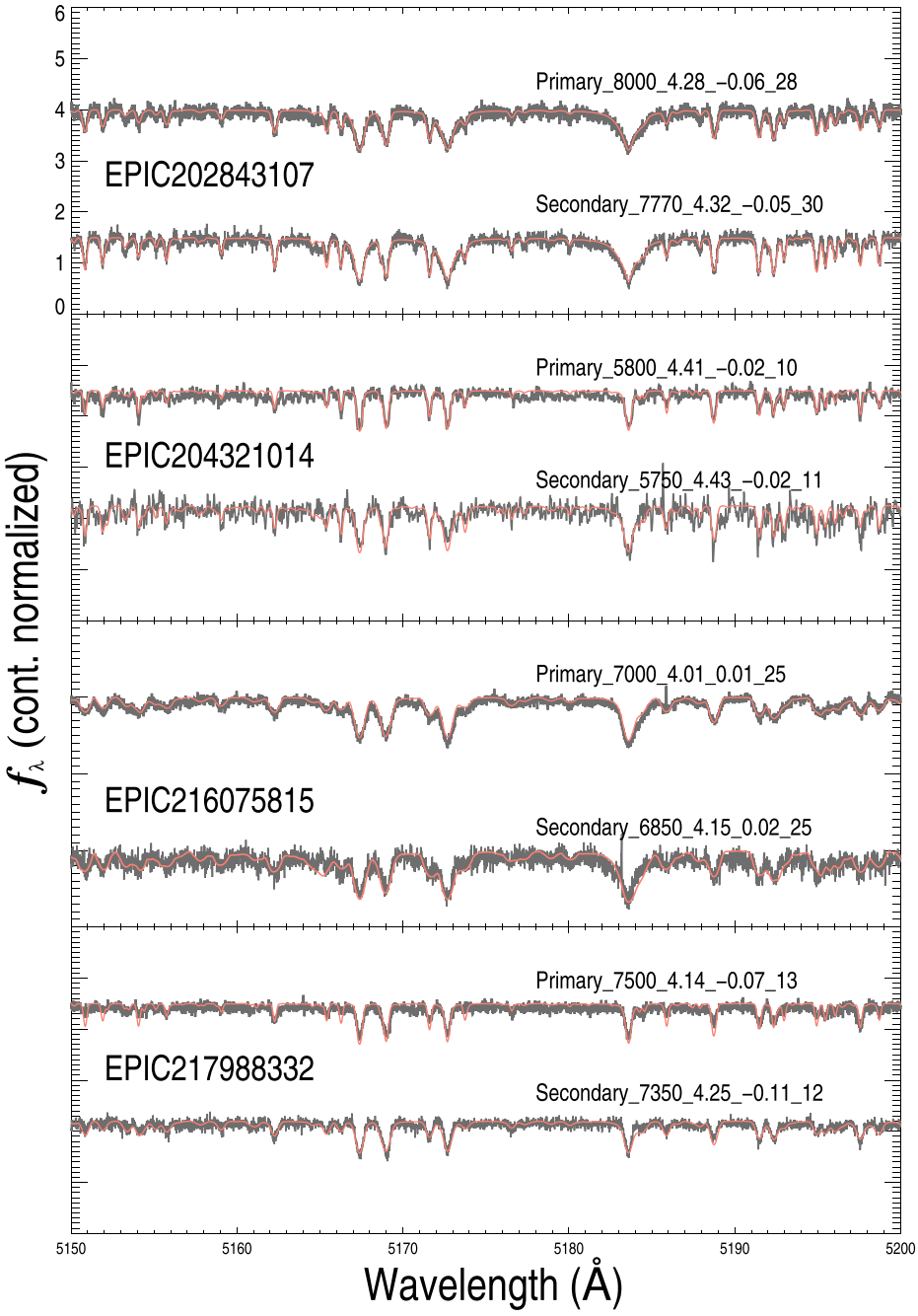

Figure 5. Illustration of the spectral disentangling procedure in the 5 150–5 200 Å wavelength region. The disentangled spectra are shown with the dark grey line. The thick red lines correspond to the model spectra with system name; `Component_`$T_{\rm eff}$`(K)_log`g`(cgs)_[M/H](dex)_v sin`i`(km s`$^{-1}$`)`.

obtained by the disentangling code, and fitted synthetic spectra of the primary and secondary components.

3.6 Reddening

Interstellar medium manifests itself as an atomic absorption line in stellar spectra like Ca, Na, and diffuse interstellar bands features. Of these structures, the Na I (D_2 at 5889.951 Å, D_1 at 5895.924 Å) line, which is the most noticeable line in the stellar spectrum, is more challenging to use for the calculation of measured interstellar extinction in the direction to each of our target stars. As we know from the observations, the measurement of reddening value is an important milestone in assigning the absolute temperature scale (and therefore the distance) of eclipsing binaries.

Munari & Zwitter (1997) empirically showed some evidence that the Na I D features are unique for tracing reddening at optically thin gas, but saturates at optically thick gas. In our study, we employed the method involved in the empirical relationship found by Munari & Zwitter (1997) that correlates reddening to the total equivalent width of the Na I D absorption lines. The equivalent width accurately measured simultaneously to several best quality spectra at quadratures, where lines from both components are unblended with

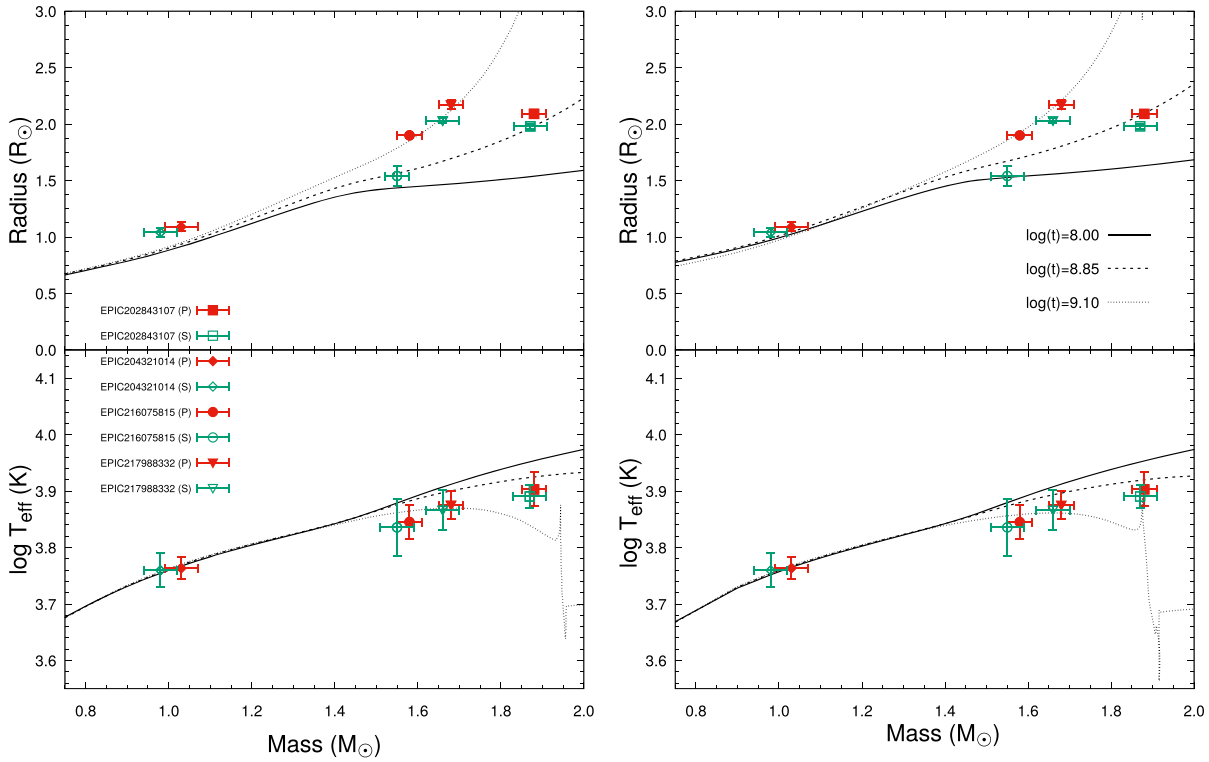

Figure 6. Comparison of the measured masses, radii, and effective temperatures of systems against stellar evolution models from the PARSEC (left) and MIST series (right) with solar-scaled metallicity. The error bars shown are the nominal values from Table 2 that do not reflect correlations discussed in the text. Dotted, dashed, and continues lines in all panels correspond to model isochrones from 0.4 to 1.2 Gyr in spaced logarithmic intervals, and the best-fitting age for each model (for PARSEC and for MIST) is indicated with the lines.

interstellar ones. The final value of $E(B-V)$ was then calculated as a sum of reddenings of individual components of each system. The results for all our investigated binaries are introduced in Table 2.

3.7 Absolute parameters

As explained prior to this section, the overall main astrophysical parameters of twin binaries obtained from the simultaneous analysis, of light curves and radial velocity were combined in order to compute the absolute values of stellar parameters using the JKTABSDIM[6] code (Southworth, Maxted & Smalley 2005). In order to compute by code the absolute parameters of the systems, the necessary input parameters are orbital period (P), eccentricity (e), fractional radii ($r_{1,2}$), velocity semi-amplitudes ($K_{1,2}$), and inclination (i) (all with formal uncertainties), and returns absolute values of masses and radii (in solar units), log (g), and rotational velocities, assuming tidal locking and synchronization. JKTABSDIM can also estimate the distance to targets, using effective temperatures of two components, measured metallicity, $E(B-V)$, and apparent magnitudes via various calibrations. The analysis results and their errors are given in Table 2. These resultant parameters were used to place the components on the Hertzsprung–Russell (HR) diagrams (Fig. 6) for the purpose of examining their evolutionary status.

4 EVOLUTIONARY STATUS

The goal of the present section is to understand the evolutionary stage, and to determine the age of the investigated systems, we made a comparison of the observed properties of the components with the PAdova and TRieste Stellar Evolution Code (PARSEC;[7] Girardi et al. 2000; Bressan et al. 2012; Chen et al. 2014) and MESA (Modules for Experiments in Stellar Astrophysics; Paxton et al. 2011, 2013, 2015, 2018) stellar evolution models in Fig. 6. The age definition of system components may then help us to enlighten on the evolutionary status of components.

One can derive the age of the examined systems generated a set of isochrones using a dedicated web interface based on the MESA and developed as part of the MESA Isochrones and Stellar Tracks project (MIST[8] ver1.2; Choi et al. 2016; Dotter 2016). For all component stars, we adopted the solar-scaled abundances that corresponds to $Y_{\odot,ini} = 0.2703$ and $Z_{\odot,ini} = 0.0142$ (Asplund et al. 2009), covering a wide range of ages, and masses, computed within a single framework. Guided by the adopted case of the consideration, we searched for the isochrones that best match the observed parameters (R, M, $T_{\rm eff}$) of each star derived in Section 3.7 and provided in Table 2.

The comparison between the absolute parameters from our analysis of light curve and radial velocity and the estimated from MESA isochrones are shown in Fig. 6 (left). In Fig. 6 (left), the positions of companions of the systems in the diagram of mass–log $T_{\rm eff}$ (K) and mass–radius ($R_\odot$) together with the isochrones from the MESA

[6]This can be obtained from https://www.astro.keele.ac.uk/jkt/codes/jktabsdim.html

[7]http://stev.oapd.inaf.it/cgi-bin/cmd

[8]http://waps.cfa.harvard.edu/MIST/interp_isos.html

binary module with solar-scaled metallicity were produced under the assumptions. It can be seen from Fig. 6 (left) that the produced models match well with the current properties of the companions of the systems. We estimated the ages of the systems to be around log (8–9) yr.

We have also fitted the components using popular and widely used sets of theoretical evolutionary models and isochrones – PARSEC. For this purpose, we used machine-readable PARSEC isochrone tables generated via the web-based tool CMD 3.3.[9] The other specificities of the code are comprehensively described in Bressan et al. (2012). Isochrones in both the mass–radius and mass–temperature diagrams are shown for the age range 0.4–1.2 Gyr in small steps, with the continuous, dashed, and dotted lines representing the best fit for the solar metallicity. As we showed from Fig. 6 (right), we pointed out an agreement in both radius and temperature at the measured masses for ages of about 0.4–1.2 Gyr, where the two confidence intervals come from the radius and temperature errors, respectively. Similarly good fits shown in the right-hand panels of the figure are found to models from the MIST models that is based on the Modules for Experiments in Stellar Astrophysics (MESA) package.

As this work is focusing on examining the agreement between the MESA and PARSEC isochrones for calculated mass, temperature, and radii of the components compared to the available isochrones, it is instructive to look at uncertainties in the fitting process and how the uncertainties in metallicity influence the final derived parameters for the components. It is essential to note that this study utilizes the isochrones themselves as being errorless: truly representing the mass and radii of stars at a given age. It seems that the stellar evolution models used to form the isochrones have uncertainties in their input parameters that influence the generated isochrones.

The binary model performed on the basis of light and radial velocity analysis with additional spectral disentangling indicate that the components of the binaries have almost the same mass. This may confirm that the components of the systems must be coeval. Due to the position of the components in the HR diagram, it could happen that while the stellar radius changes expeditiously, each components will spend the main sequence evolution phase together. As we know from the theoretical stellar evolutionary models, a negligible mass difference can result in a large radius difference. Having shown how stellar parameters are calculated with different methods (Table 2), these differences may be seen in the panel of Fig. 6 clearly. Because of their specific and well-defined evolutionary status EPIC 202843107, EPIC 216075815, and EPIC 217988332 are interesting cases, as both components in these systems are possible pulsating. At least, we expect the components to pulsate based on their location being inside the theoretical δ Sct and γ Dor instability strip to within the error bars.

It is also interesting to note the existence of discrepancies in the derived age between primary and secondary components of EPIC 216075815. The evolutionary status of twin stars such as EPIC 216075815 has been a subject of debate for decades. While it can be clearly seen from Fig. 6 that the hotter primary is crossing the log $(t) = 9.1$ Gyr isochrone and the secondary components are approaching the log $(t) = 8.85$ Gyr isochrone, opinions have varied on the precise location of the components, in large part because of uncertainties in the radius as well as the effective temperatures used to place the star on the diagram. An equivalent way of interpreting the discrepancy is in terms of the lower S/N ratio of the HARPS spectra. The hotter star is better disentangled due to a higher light contribution to the spectra than the secondary component, the difference being about 15 per cent, as seen more clearly in Fig. 2. As mentioned above, EPIC 216075815 is perhaps unique in that, in addition to those twin properties, it is a candidate for being a γ Dor pulsator. Unfortunately, neither twin nor eclipsing binaries are common, so the chance of finding such an unusual pair seems incredibly rare.

[9] http://stev.oapd.inaf.it/cgi-bin/cmd

5 NOTEWORTHY PULSATING COMPONENTS IN ECLIPSING BINARIES

Most types of pulsating stars have recently gained more attention. Pulsating stars were also found in eclipsing binary systems, but for various reasons, this type of star is more difficult to analyse. In all but one case, pulsating components in eclipsing binaries, characterized by pulsating amplitudes, cause the modelling to be extra intricate. However, pulsating components in eclipsing binaries are widely recognized as a very good tool for studying the pulsating mechanisms and for the understanding of fundamental physics of the stars.

According to the results of the spectroscopic and light curves analyses of twin binaries and from their position in HR diagram, the primary and/or secondary stars of EPIC 217988332 and EPIC 202843107 would be a candidate for δ Sct and EPIC 216075815 would be a candidate γ Dor pulsators. Both the primary and secondary components of the studied systems have stellar characteristics similar to the pulsating-type stars (i.e. mass and temperature) therefore the following analyses and results concern the pulsating nature of the components.

To detect oscillations, high-precision and continuous observations are essential. The main difficulty in searching for oscillations in the light-curve data of our samples is that every pulsation frequency in the Fourier spectrum is accompanied by many aliases, reflected around integer multiples of the sampling frequency. To figure out pulsating signatures, we apply the discrete Fourier transform code SIGSPEC (Reegen 2007) to a set of light curves from *K2* to perform a frequency analysis of linearly interpolated gapped light curves. SIGSPEC calculates the spectral significance levels in an iterative process, by using a combination of discrete Fourier transform and least-squares fitting algorithms, to extract the frequencies, amplitudes, and phases of multiperiodic signals of a time series at a randomly given sampling. The analysis with SIGSPEC yielded formally significant frequencies with S/N values higher than 5.0 (spectral significance parameter; $\sigma = 5.5$ proposed by Reegen (2007) as *theoretically* equivalent of S/N = 4.0). Applying the significance thresholds given above, SIGSPEC finds formally significant frequencies for the *K2* long-cadence residual data. Table 3 contains the values of the linear combination and unique frequencies found for each system. The errors of all values listed in Table 3 are derived according to Kallinger, Reegen & Weiss (2008).

5.1 EPIC 202843107

In order to analyse the pulsation characteristics of this binary system in detail, we performed a frequency analysis of the residual data around phases 0.0 and 0.5 that was masked because the binary components block each other during eclipses. The data defined from the outside-eclipse with phases 0.02–0.45 and 0.51–0.98 was subjected to frequency analysis using the SIGSPEC code. The code has been repeated until no significant frequency peaks were found above the confidence level in the residuals. The light residuals after removing the binary effects from the observed data are plotted in Fig. 7 (upper panel) as mmag versus BJD, where the insets panels present a short section of the residuals. From our detailed analyses, we found 29 frequencies with the criterion of the code; this could

Table 3. Oscillation frequencies for the pulsating components of all systems.

ID	Frequency (μHz)	Amplitude (mmag)	Phase (rad)	rms	Linear combinations
			EPIC 202843107		
f_1	208.77(2)	0.54(10)	3.55(05)	0.010145	
f_2	176.76(2)	0.47(10)	1.20(05)	0.009140	
f_3	192.43(2)	0.43(11)	2.72(05)	0.008323	
f_4	2.62(3)	0.25(17)	1.22(08)	0.007599	$\sim f_{\rm orb}$
f_5	230.36(3)	0.22(17)	1.05(08)	0.007349	
f_6	5.27(3)	0.26(16)	5.66(08)	0.007097	$2f_{\rm orb}$
f_7	171.36(3)	0.22(17)	1.45(08)	0.006841	$f_2 - 2f_{\rm orb}$
f_8	231.92(4)	0.15(23)	5.10(11)	0.006618	
f_9	151.02(4)	0.14(24)	2.50(11)	0.006505	$f_1 + f_2 - f_{\rm orb} - f_8$
f_{10}	165.87(5)	0.12(28)	4.46(13)	0.006405	
f_{11}	207.43(5)	0.11(30)	6.10(14)	0.006327	
f_{12}	257.01(6)	0.09(35)	3.72(16)	0.006261	$3f_1 - f_2 - f_3$
f_{13}	161.08(6)	0.09(36)	3.84(17)	0.006213	$2f_2 - f_3$
f_{14}	227.72(6)	0.09(38)	2.76(18)	0.006168	$-f_{orb} + f_5$
f_{15}	27.67(7)	0.08(40)	4.22(19)	0.006129	$-2f_1 + f_2 - f_3 + 2f_5$
f_{16}	55.68(7)	0.08(41)	3.79(19)	0.006093	$f_1 - 2f_3 + f_8$
f_{17}	8.58(7)	0.08(40)	4.05(19)	0.006059	$-f_1 + f_2 - f_3 + f_{\rm orb} + f_5$
f_{18}	83.34(7)	0.08(41)	4.73(19)	0.006024	
f_{19}	199.20(7)	0.08(41)	3.58(19)	0.005991	$2f_2 - f_3 + f_5$
f_{20}	131.96(7)	0.08(41)	1.03(19)	0.005957	$2f_1 + f_2 - f_5 - f_8$
f_{21}	5.94(7)	0.07(41)	5.11(19)	0.005925	$-f_1 + f_2 - f_3 + f_5$
f_{22}	174.27(7)	0.07(41)	0.18(19)	0.005892	$f_2 - f_{\rm orb}$
f_{23}	16.81(7)	0.07(41)	0.32(19)	0.005860	
f_{24}	28.84(7)	0.10(42)	3.37(19)	0.005828	$-2f_2 + 2f_3 - f_{\rm orb}$
f_{25}	12.79(7)	0.10(42)	3.08(19)	0.005797	$-2f_3 + f_8 + f_{10}$
f_{26}	18.34(7)	0.08(43)	2.47(20)	0.005766	
f_{27}	2.42(7)	0.08(42)	6.18(20)	0.005734	
f_{28}	12.89(7)	0.12(40)	1.05(19)	0.005704	$-f_2 + f_3 - f_{\rm orb}$
f_{29}	19.49(7)	0.07(44)	0.16(20)	0.005666	$f_2 - 2f_3 - f_{\rm orb} + f_5$
			EPIC 216075815		
f_1	0.153(14)	0.19(10)	4.91(5)	0.004600	
f_2	0.426(15)	0.27(10)	5.00(5)	0.004187	$2f_1$
f_3	0.806(17)	0.22(12)	2.39(6)	0.003833	
f_4	2.437(16)	0.15(11)	4.06(5)	0.003598	
f_5	0.573(18)	0.22(12)	0.54(6)	0.003347	$-f_1 + f_3$
f_6	0.943(15)	0.16(10)	1.43(5)	0.003087	f_3
f_7	3.318(21)	0.10(15)	0.66(7)	0.002822	$f_3 + f_4$
f_8	2.305(20)	0.15(14)	3.57(7)	0.002712	f_4
f_9	2.068(22)	0.10(15)	1.18(7)	0.002598	$-2f_1 + f_4$
f_{10}	2.983(22)	0.28(15)	0.16(7)	0.002495	$-f_1 + f_3 + f_4$
f_{11}	4.336(25)	0.05(17)	5.31(8)	0.002392	$f_1 + 2f_3 + f_4$
f_{12}	5.542(26)	0.17(18)	3.76(8)	0.002328	
f_{13}	14.485(25)	0.06(18)	2.67(8)	0.002268	
...	...	...	...	...	...
f_{49}	31.874(51)	0.02(36)	4.94(17)	0.001288	
...	...	...	...	...	...

be due to the quality of the data. The synthetic curve calculated from the 29-frequency fit is overplotted as a solid curve in the same figure. In the lower panel of Fig. 7, the amplitude spectrum of the residuals is presented with significant frequencies marked in the amplitude periodorgam with dotted lines. The output of the runs is given in Table 3, where the significant frequencies are enumerated in order of decreasing amplitude, and the uncertainties are calculated as proposed by Kallinger et al. (2008).

As can be seen in Fig. 7 and Table 3, dominant pulsational frequencies cluster in the range of 2–21 d^{-1} for EPIC 202843107. We found nearly credible periodicity near the $f_{1...8}$ frequencies calculated by Ou et al. (2019).

Table 3 shows the frequencies, amplitudes, phases, and linear combinations for the peaks seen in Fig. 7. For the first estimate of mode identification, it is useful to look at the Q value for each of the well-defined frequencies. This is defined to be $Q = P_{\rm puls}\sqrt{\frac{\overline{\rho}}{\overline{\rho}_\odot}}$ where $P_{\rm puls}$ is the pulsation period and $\overline{\rho}$ is the mean density; Q is known as the 'pulsation constant'. Standard values for δ Sct models are $Q = 0.033$ for the fundamental mode and 0.025 for the first overtone (Stellingwerf 1979). There is an interesting possibility to determine the average density of the primary star by using the pulsation constant. This method is most useful for pulsating stars in eclipsing binaries, where the density of the stars can be determined accurately from the light-curve analysis. Adopting $\overline{\rho}_\odot$ ($\overline{\rho}_\odot = 1.408$ g cm^{-3}) and Q values, we calculated the average density of the primary component as $\overline{\rho} = 0.286331 \pm 0.000005\ g\ cm^{-3}$. The resulting $\overline{\rho}$ is consistent with $\overline{\rho}_{LC} = 0.290 \pm 0.013$ g cm^{-3} derived from light-curve analysis explained in the previous section, thus suggesting that the mode so far examined is exists. It is nevertheless proof that additional pulsation mode frequencies of low amplitude that are not seen at the scale of the data can exist. Those will be examined in detail in a future study with high-quality data.

5.2 EPIC 217988332

EPIC 217988332 is composed of two nearly identical mass stars ($M \approx 1.67\,M_\odot$) on a 6.5-d non-eccentric orbit ($e \approx 0.0$). Based on their location in the HR diagram we expected only one of the components to pulsate. Their power spectrum clearly suggests the system is non-oscillating, and indeed, we have no other evidence for pulsating modes.

Guzik et al. (2015) and Murphy et al. (2015) focused on causes of lack of modes, as a new perspective of pulsation in stars within the δ Scuti instability strip recently emerged as a result of *Kepler* observations. They also inferred that the δ Scuti instability strip is *pure* despite the existence of the basic question whether there are non-variable stars in the strip. EPIC 217988332 can be considered an important source for other *constant* stars within this framework.

5.3 EPIC 216075815

Considering our absolute parameters presented in the previous section, both components of the system reside inside the γ Dor instability strip in the HR diagram, whose oscillations are driven by convective flux blocking (Guzik et al. 2000). One of the presented systems in this work, EPIC 216075815, is sufficiently hot (Fig. 4) to be a γ Dor star. The *K2* long-cadence data set out total eclipses and oscillations at the secondary minima. These show that the smaller secondary star is completely eclipsed by its nearly twin primary and the primary star is the main source of the light variations.

In order to obtain the light curve we have downloaded the target pixel file pertaining to this star from the MAST[10] database. Subsequently, we produced our own mask and using the KEPEXTRACT routine inside the PYKE tools (Still & Barclay 2012) we have extracted the light curve. After the loss of the two reaction wheels of the *Kepler Space Telescope*, aiming stability is achieved by firing the thrusters periodically every ~6.5 h. These periodic operations cause deformations on the obtained light curves. Prior to the light-curve analyses these deformations were substantially corrected by using the KEPSFF routine in PYKE tools. The low frequency level variations were also corrected with the KEPFLATTEN routine in the same manner. The remaining outliers, then, were extracted manually. The corrected (final) light curve was again solved by the PHOEBE , in order to obtain the theoretical light curve of the system's orbital motion. Then, this theoretical light curve is subtracted from the observed light curve to obtain the residual light curve and the data that resides in eclipse

[10]This can be obtained from https://archive.stsci.edu/

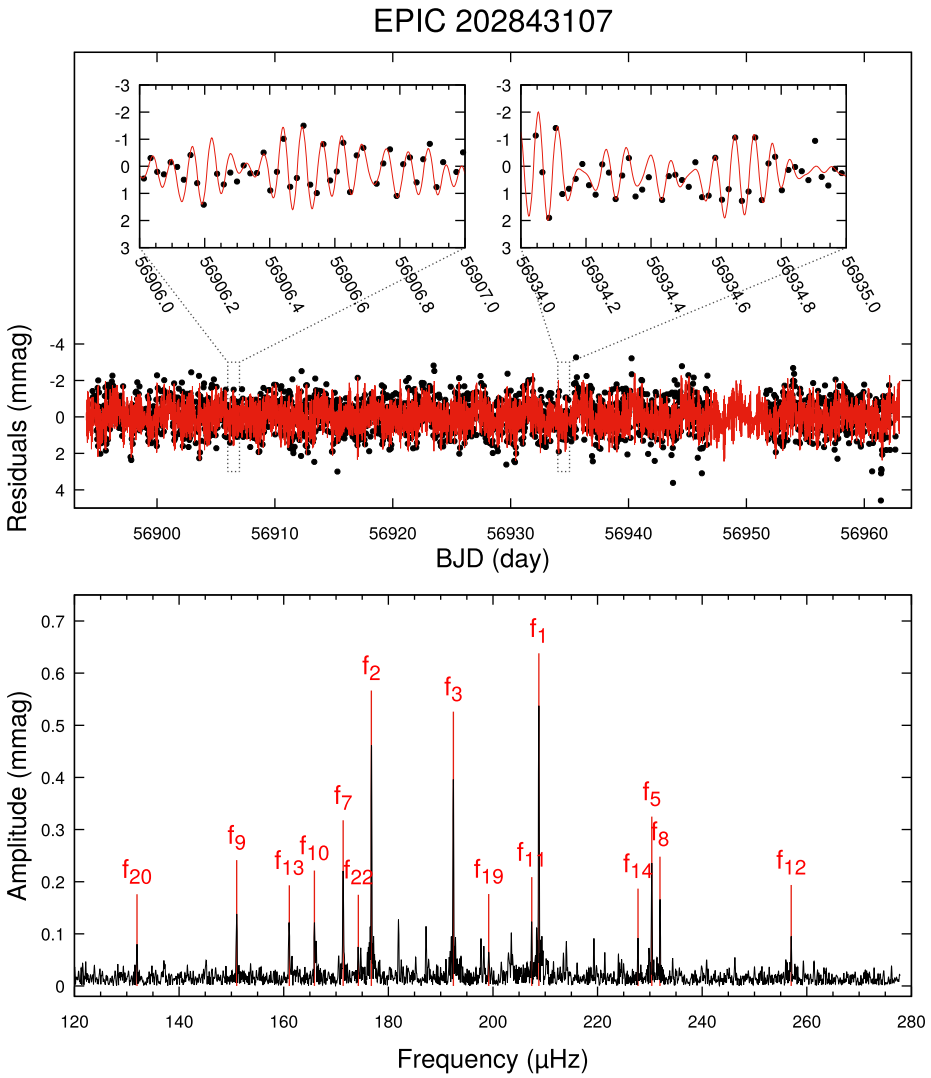

Figure 7. The upper panel presents light-curve residuals after removing the binarity effects from the observed data and a short section of the residuals marked by the inset box. The synthetic curve is computed from the 29-frequency fit to the data. The lower panel presents the 15 dominant frequencies listed in Table 3.

phases is removed. The final data was Fourier analysed with the SIGSPEC code to obtain the pulsation frequencies. The light residuals, after removing the binary effects from the observed data, are plotted in Fig. 8 (upper panel) as mmag versus BJD, where the insets panels present a short section of the residuals. From our detailed analyses, we found 69 frequencies with the criterion of the code, this could be due to the quality of the data. The synthetic curve calculated from the 69-frequency fit is overplotted as solid curve in same figure. In the lower panel of Fig. 8, the amplitude spectrum of the residuals is presented with significant frequencies marked in the amplitude periodorgam with dotted lines. The output of the runs is given in Table 3, where the significant frequencies are enumerated in order of decreasing amplitude.

Since the secondary eclipse is a total one, we decided to repeat the analysis while also adding the secondary eclipse data. The phases of the minimum cannot be represented equally well enough compared to the maximum phases in the PHOEBE solution. For this reason, observed theoretical residuals could not be generated. However, a linear fit was applied to the total eclipse phase data (0.49–0.51). The residuals of the observed data-linear fit are combined with the previously obtained SIGSPEC data and the solution was repeated. Finally, it was seen that the results of both solutions are similar to each other. The results from this process are plotted in Fig. 8 with (blue) square symbols.

According to the successive prewhitening, we have known that EPIC 216075815 pulsator displays strong changes, where the pulsation amplitude scan varies by several factors or more. However, it may also be the case that the pulsating nature of star in the system is affecting the light curve more than we expect. Given the fact that we were not able to obtain a perfect fit for the residuals, there is a systematic error in the light curve that is difficult to assess before improved best mode search becomes available.

6 SUMMARY AND CONCLUSIONS

We have examined the photometric and spectroscopic analysis to study the binarity and pulsation nature of the twin eclipsing binaries based mainly on the *Kepler* and high resolution spectroscopic data. Certain physical parameters of the binary systems were determined. Using the physical parameters of the components obtained from

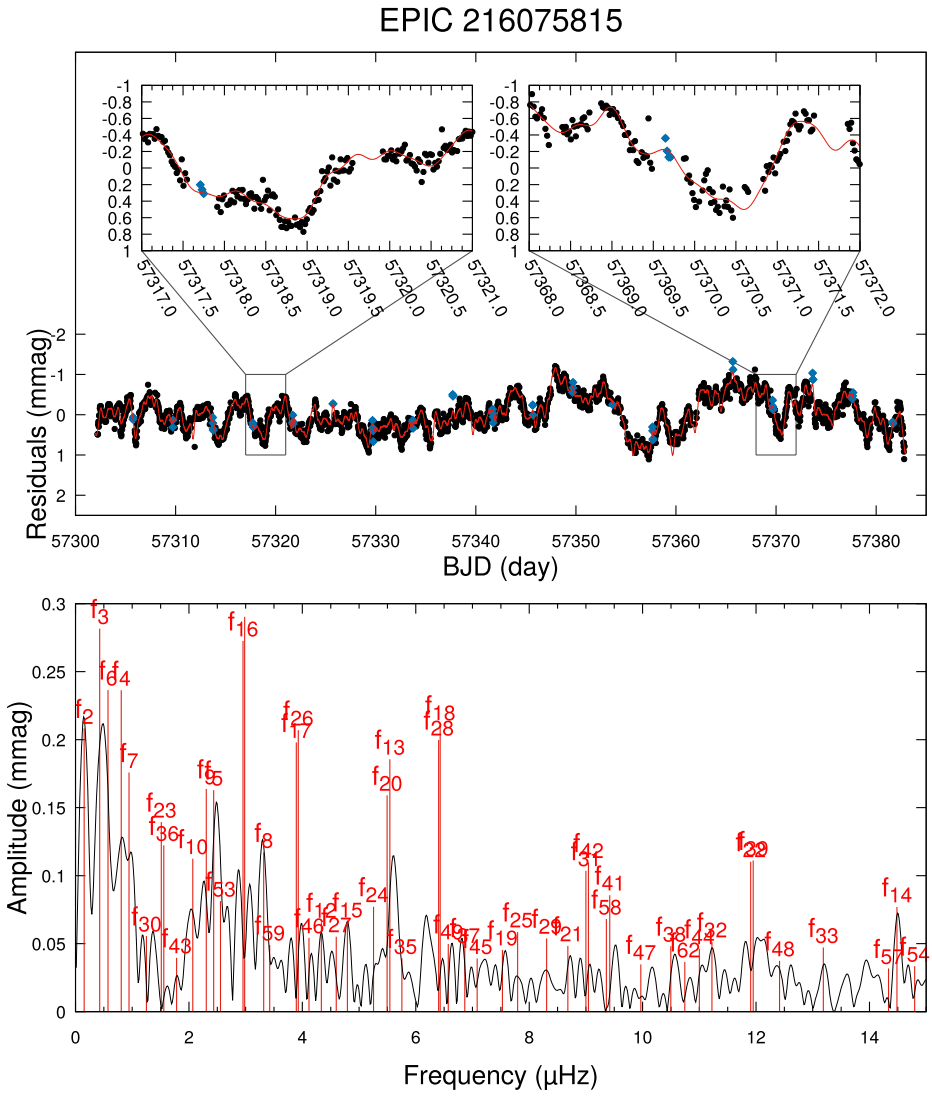

Figure 8. The upper panel presents light-curve residuals after removing the binarity effects from the observed data and a short section of the residuals marked by the inset box (blue square symbols are explained in Section 5.3). The synthetic curve is computed from the 69-frequency fit to the data. The lower panel presents the 52 dominant frequencies listed in Table 3.

photometric and spectroscopic data, the resultant evolutionary status and dynamic properties from binary modelling indicate that three of these systems lie within the instability strip. We did find a system composed of two nearly identical mass stars (EPIC 217988332) that appear to be twin, does not pulsate, and lies in the middle of the δ Scuti instability strip, albeit in the main sequence evolutionary phase. This star is similar to its kind confirmed by Guzik et al. (2015). As far as we know, none of the pulsation mechanisms gives a satisfactory explanation of the pulsation nature of the system. Thus, it indicates that the star type is rare.

The systems investigated in this study are also precious test cases to determine the level to which twin binaries are physically identical or fraternal and how the systems are shaped chemically. With respect to the chemical tagging investigation one would anticipate no distinctions in the observed abundance ratios ([X/H] or [X/Fe]) measured in both components of a twin binary system born from the same gas cloud.

For distance determination to the systems, we adopted interstellar reddening of $E(B-V)$s as derived from the correlation reddening of the total equivalent width of the Na I D absorption lines. Subsequently, the average distance calculated for systems was in good agreement with EPIC 216075815 and EPIC 217988332 as calculated with the trigonometric parallax from the eDR3 (Gaia Collaboration 2016, 2020). The average distances reported in eDR3 for the EPIC 202843107 and EPIC 204321014 are inconsistent with the ones derived from our distance estimation. The Gaia distance is only about 80 per cent of this value and our results are formally inconsistent with eDR3. The inconsistency may be due to unreliable distance-extinction estimates or the positioning of the systems such that no star is sufficiently isolated to allow a reliable parallax determination. To confirm which distance is the correct one, individual astrometric measurements should be released and binary orbits are included in the fits, which can be expected from future data releases.

Hawkins et al. (2020) used a large sample of main sequence stars extracted from the second data release *Gaia* DR2, to study the chemical tagging properties of identical and fraternal binaries that might be chemically homogeneous in [Fe/H]; however, other

elements were still in question. This result remains a formidable challenge for twin binaries.

Critically, pulsating components of binary systems have been partially affected from orbital and pulsation periods, as well as a correlation between evolutionary status and dominant pulsation frequency likely to occur (Liakos et al. 2012). However, we do not have enough samples to know; the pulsating component of twin binaries may differ regarding their evolutionary status. Therefore, twin binary members and binary-contained pulsating stars, although they present similar pulsational properties, should not be considered of the identical type due to a likely different evolutionary past. Future space missions such as *Gaia* and *TESS* are expected to increase the current samples of binaries containing components similar to each other to better test possible dependence of the physical characteristics, chemical tagging, and pulsational behaviour on the evolutionary history.

Moreover, a physical interpretation of the empirical relations correlating the pulsation and absolute parameters of twin binary components with the evolutionary stage of the components is certainly needed. Future theoretical modelling for twin binary systems should take into account quantities such as equal mass, radius, radius expansion rate, and affecting the dominant pulsation period. Hence, the combination of theoretical models and current observational results is expected to answer a lot of open questions, enriching our knowledge about the evolutionary status of twin binaries at the end of the main sequence phase and beyond.

ACKNOWLEDGEMENTS

We are grateful to the anonymous referee for her/his valuable suggestions. This research made use of data collected at ESO under programmes 099.D-0380(A), 0100.D-0273(A) (by Gieren, W.) and 0101.D-0697(A) (by Pietrzynski, G.). We thank Ege University Research Foundation (Project No. FDK-2019-20215) for supporting this study. This article is a part of the PhD thesis of BH. The following internet-based resources were used in research for this paper: the NASA Astrophysics Data System; the SIMBAD database operated at CDS, Strasbourg, France. This work is based on data from the *Kepler* mission. *Kepler* was competitively selected as the tenth Discovery mission. Funding for this mission is provided by NASA Science Mission Directorate. The photometric data were obtained from the Mikulski Archive for Space Telescopes (MAST). This work has also made use of data from the European Space Agency (ESA) mission *Gaia* (http://www.cosmos.esa.int/gaia), processed by the *Gaia* Data Processing and Analysis Consortium (DPAC, http://www.cosmos.esa.int/web/gaia/dpac/consortium).

DATA AVAILABILITY

The data underlying this article will be shared on reasonable request to the corresponding author.

REFERENCES

Armstrong D. J. et al., 2016, MNRAS, 456, 2260
Asplund M., Grevesse N., Sauval A. J., Scott P., 2009, ARA&A, 47, 481
Barros S. C. C., Demangeon O., Deleuil M., 2016, A&A, 594, A100
Blanco-Cuaresma S., Soubiran C., Heiter U., Jofré P., 2014, A&A, 569, A111
Borucki W. J. et al., 2010, Science, 327, 977
Bressan A., Marigo P., Girardi L., Salasnich B., Dal Cero C., Rubele S., Nanni A., 2012, MNRAS, 427, 127
Chen Y., Girardi L., Bressan A., Marigo P., Barbieri M., Kong X., 2014, MNRAS, 444, 2525
Choi J., Dotter A., Conroy C., Cantiello M., Paxton B., Johnson B. D., 2016, ApJ, 823, 102
Dotter A., 2016, ApJS, 222, 8
El-Badry K., Rix H.-W., Tian H., Duchêne G., Moe M., 2019, MNRAS, 489, 5822
Gaia Collaboration et al., 2016, A&A, 595, A1
Gaia Collaboration, Brown A. G. A., Vallenari A., Prusti T., de Bruijne J. H. J., Babusiaux C., Biermann M., 2020, A&A, preprint (arXiv:2012.01533)
Girardi L., Bressan A., Bertelli G., Chiosi C., 2000, A&AS, 141, 371
Gray D. F., 2005, The Observation and Analysis of Stellar Photospheres, 3rd edn. Cambridge Univ. Press, Cambridge
Gray R. O., Corbally C. J., 1994, AJ, 107, 742
Gray R. O., Corbally C. J., 2009, Stellar Spectral Classification. Princeton University Press, Princeton
Grevesse N., Asplund M., Sauval A. J., 2007, SSRv, 130, 105
Gustafsson B., Edvardsson B., Eriksson K., Jørgensen U. G., Nordlund Å., Plez B., 2008, A&A, 486, 951
Guzik J. A., Kaye A. B., Bradley P. A., Cox A. N., Neuforge C., 2000, ApJ, 542, L57
Guzik J. A., Bradley P. A., Jackiewicz J., Molenda-Zakowicz J., Uytterhoeven K., Kinemuchi K., 2015, Astron. Rev., 11, 1
Hadrava P., 1995, A&AS, 114, 393
Halbwachs J. L., Mayor M., Udry S., Arenou F., 2003, A&A, 397, 159
Hawkins K. et al., 2020, MNRAS, 492, 1164
Hensberge H., Ilijić S., Torres K. B. V., 2008, A&A, 482, 1031
Howell S. B. et al., 2014, PASP, 126, 398
Huber D. et al., 2016, ApJS, 224, 2
Høg E. et al., 2000, A&A, 355, L27
Ilijic S., 2004, in Hilditch R. W., Hensberge H., Pavlovski K., eds, ASP Conf. Ser. Vol. 318, Spectroscopically and Spatially Resolving the Components of the Close Binary Stars. Astron. Soc. Pac., San Francisco, p. 107
Ilijic S., Hensberge H., Pavlovski K., Freyhammer L. M., 2004, in Hilditch R. W., Hensberge H., Pavlovski K., eds, ASP Conf. Ser. Vol. 318, Spectroscopially and Spatially Resolving the Components of the Close Binary Stars. Astron. Soc. Pac., San Francisco, p. 111
Kallinger T., Reegen P., Weiss W. W., 2008, A&A, 481, 571
Kirk B. et al., 2016, AJ, 151, 68
Kurucz R. L., 1993, ATLAS9 Stellar Atmosphere Programs and 2 km/s grid., Kurucz CD-ROM No. 13. Smithsonian Astrophysical Observatory, Cambridge
Liakos A., Niarchos P., Soydugan E., Zasche P., 2012, MNRAS, 422, 1250
Lombardi J. C., Holtzman W., Dooley K. L., Gearity K., Kalogera V., Rasio F. A., 2011, ApJ, 737, 49
Lucy L. B., 1967, Zeit. für Astrophysik, 65, 89
Lucy L. B., 2006, A&A, 457, 629
Lucy L. B., Ricco E., 1979, AJ, 84, 401
Maxted P. F. L., Hutcheon R. J., 2018, A&A, 616, A38
Mazeh T., Zucker S., 1994, Ap&SS, 212, 349
Mochnacki S. W., 1984, ApJS, 55, 551
Munari U., Zwitter T., 1997, A&A, 318, 269
Murphy S. J., Bedding T. R., Niemczura E., Kurtz D. W., Smalley B., 2015, MNRAS, 447, 3948
Ou J.-W., Yang M., Zhou J.-L., 2019, RAA, 19, 112
Paxton B., Bildsten L., Dotter A., Herwig F., Lesaffre P., Timmes F., 2011, ApJS, 192, 3
Paxton B. et al., 2013, ApJS, 208, 4
Paxton B. et al., 2015, ApJS, 220, 15
Paxton B. et al., 2018, ApJS, 234, 34
Penny L. R. et al., 2001, ApJ, 548, 889
Pilecki B. et al., 2013, MNRAS, 436, 953
Pilecki B. et al., 2015, ApJ, 806, 29
Prša A., Zwitter T., 2005, ApJ, 628, 426
Prša A. et al., 2011, AJ, 141, 83
Reegen P., 2007, A&A, 467, 1353
Ruciński S. M., 1969, Acta Astron., 19, 245

Rucinski S. M., 2002, AJ, 124, 1746
Ryabchikova T., Piskunov N., Kurucz R. L., Stempels H. C., Heiter U., Pakhomov Y., Barklem P. S., 2015, Phys. Scr., 90, 054005
Sheminova V. A., 2019, Kinemat. Phys. Celest. Bodies, 35, 129
Simkin S. M., 1974, A&A, 31, 129
Simon K. P., Sturm E., 1994, A&A, 281, 286
Simon M., Obbie R. C., 2009, AJ, 137, 3442
Sing D. K., 2010, A&A, 510, A21
Southworth J., Maxted P. F. L., Smalley B., 2005, A&A, 429, 645
Stellingwerf R. F., 1979, ApJ, 227, 935
Still M., Barclay T., 2012, Astrophysics Source Code Library, record ascl:1208.004
Tokovinin A. A., 2000, A&A, 360, 997
Tonry J., Davis M., 1979, AJ, 84, 1511
Topping J., 1972, Errors of Observation and Their Treatment, 4th edn. Chapman and Hall Ltd., London
Vanderburg A., Johnson J. A., 2014, PASP, 126, 948
Wilson R. E., 1979, ApJ, 234, 1054
Wilson R. E., Devinney E. J., 1971, ApJ, 166, 605

APPENDIX A: RADIAL VELOCITY MEASUREMENTS OF TARGETS

Table A1. Journal of the radial velocity measurements of the targets.

System	BJD (+2400000)	v_1 (km s^{-1})	σ_1 (km s^{-1})	v_2 (km s^{-1})	σ_2 (km s^{-1})	S/N[a]	Instrument
EPIC 202843107	57 915.6003	− 147.4	0.3	52.9	0.2	16.7	HARPS
	57 916.6142	− 71.7	0.4	− 22.2	0.5	4.6	HARPS
	58 146.8630	44.7	0.3	− 140.0	0.2	21.4	HARPS
	58 148.8457	− 147.5	0.2	52.8	0.2	18.5	HARPS
	58 232.8137	− 125.6	0.2	31.0	0.2	16.6	HARPS
	58 247.8489	51.2	0.2	− 147.6	0.2	13.4	HARPS
EPIC 204321014	58 148.8111	97.9	0.2	− 65.7	0.2	21.1	HARPS
	58 233.6551	− 17.6	0.2	55.8	0.2	19.9	HARPS
	58 433.4551	102.6	0.2	− 70.2	0.2	33.3	HARPS
	58 613.6551	− 66.2	0.2	106.2	0.2	31.3	HARPS
EPIC 216075815	57 914.27964	65.6	0.1	− 25.8	0.3	20.9	HARPS
	57 915.23185	− 57.5	0.1	105.1	0.3	17.9	HARPS
	57 915.42808	− 70.4	0.1	118.0	0.2	23.6	HARPS
	57 916.20754	− 31.9	0.1	78.1	0.2	20.0	HARPS
	57 916.41286	− 5.4	0.1	49.5	0.3	22.6	HARPS
	58 233.24107	114.8	0.1	− 78.6	0.2	18.2	HARPS
	58 233.41519	113.2	0.1	− 75.8	0.2	10.4	HARPS
	58 247.40558	− 69.5	0.1	118.8	0.2	11.4	HARPS
EPIC 217988332	57 915.7419	− 67.3	0.2	20.6	0.2	43.2	HARPS
	57 915.9330	− 79.2	0.2	33.5	0.2	30.2	HARPS
	58 232.8871	4.9	0.2	− 50.8	0.2	19.1	HARPS
	58 247.9082	− 108.2	0.2	61.8	0.2	14.0	HARPS

[a]S/N values have been obtained from headers.

This paper has been typeset from a TEX/LATEX file prepared by the author.